e-J. Surf. Sci. Nanotech. Vol. 7 (2009) 161-166 Conference - ISSS-5 -

Effects of Surface Stress on Nanocantilevers*

H. Sadeghian†
Structural Optimization and Computational Mechanics (SOCM) group, Department of Precision and Microsystems Engineering, Delft University of Technology, The Netherlands, and Electronic Instrumentation Laboratory, Department of Microelectronics, Delft University of Technology, The Netherlands,

C. K. Yang
Electronic Instrumentation Laboratory, Department of Microelectronics, Delft University of Technology, The Netherlands,

K. Babaei Gavan
Kavli Institute of Nanoscience, Delft University of Technology, The Netherlands,

J. F. L. Goosen
Structural Optimization and Computational Mechanics (SOCM) group, Department of Precision and Microsystems Engineering, Delft University of Technology, The Netherlands,

E. W. J. M. van der Drift and H. S. J. van der Zant
Kavli Institute of Nanoscience, Delft University of Technology, The Netherlands

P. J. French and A. Bossche
Electronic Instrumentation Laboratory, Department of Microelectronics, Delft University of Technology, The Netherlands

F. van Keulen
Structural Optimization and Computational Mechanics (SOCM) group, Department of Precision and Microsystems Engineering, Delft University of Technology, The Netherlands

(Received 7 November 2008; Accepted 2 February 2009; Published 14 March 2009)

Surface and interface effects play significant roles in mechanical properties of nanostructures. Traditional continuum mechanics does not account for surface and interface effects on the elastic behavior of nanostructures. This work presents a general Lagrangian mechanics framework to describe the surface elastic properties. This model includes the surface effects on overall elastic behavior of a nanocantilever. It is demonstrated that the overall elastic behavior of the nanostructures is scale-dependent. Silicon nanocantilever have been fabricated with dimensions from 200 to 8 μm length, 25 to 4 μm width and 1 μm, 340 nm, and 93 nm thicknesses. The resonance behavior is studied and is compared with resonance frequency measurement in order to see at which scale other surface effects become significant. [DOI: 10.1380/ejssnt.2009.161]

Keywords: Surface stress; Nanocantilever; Scale-dependent

I. INTRODUCTION

Recently, interest in utilizing very small resonant cantilevers as physical, chemical, or biological sensor to dynamically detect a targeted substance has increased very rapidly [1–3]. Research on resonant cantilever sensors has focused on improving their sensitivity by scaling down or modifying their structural configuration. It has been reported that their sensitivity can be enhanced such that it is possible to count molecules. Piezoelectric resonant microcantilever possessing a mass sensitivity in the femtogram/Hz regime, as a typical example, is presented in [4], allowing a single virus to be detected. The resonance frequency shift and the deflection as a function of adsorption are two main transduction mechanisms for microcantilever sensors [5, 6, 8]. However, it has recently been reported that the resonant frequency of a cantilever sensor is also affected by surface stresses induced by adsorption. It was found that the surface stress affects the overall stiffness of a cantilever which affects the resonance frequency [7, 9]. In addition, many models have been proposed to explain adsorption-induced surface stress change and its resultant resonance frequency shift or detection of a microcantilever in vacuum or in gaseous environment [6, 10–14].

Previous theoretical studies concerning surface stress-induced change of submicron cantilever behavior have followed the treatment given by Chen *et al.* [6]. In that paper the problem of a self-balanced cantilever deformation due to adsorption without any external forces has been replaced by a problem of bending or vibration of the cantilever under an applied force. Although a taut string model [6] and a beam with axial force [15, 16] have been suggested, neither approach represents the physics correctly. The effective external forces are considerably

* This paper was presented at International Symposium on Surface Science and Nanotechnology (ISSS-5), Waseda University, Japan, 9-13 November, 2008.

†Corresponding author: H.SadeghianMarnani@tudelft.nl

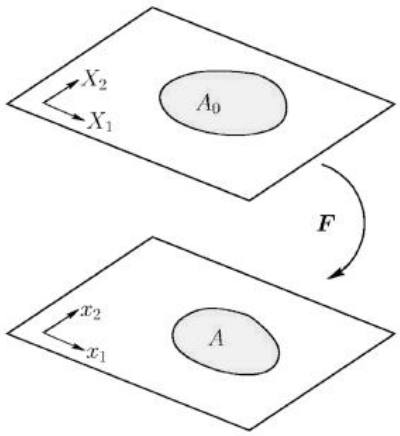

FIG. 1: Surface under homogeneous deformation.

overestimated, because in the real situation the cantilever has a free end to allow deformation or bending to relieve the stress resultant and stress couples.

In this paper a description of surface stress induced-changes in stiffness of nanocantilever is proposed instead. The stiffness change due to surface stress is used to calculate the resonance frequency of nanocantilevers. The predicted resonance frequency is compared with measured data to study for which thicknesses the other effects like surface oxidation, water and gas adsorption become significant.

II. CONTINUUM DESCRIPTION OF SURFACE PROPERTIES

The aim of this section is to develop a Lagrangian description that includes the surface stress effects. As shown in Fig.1, the initial and deformed position of a continuum surface is denoted by $\mathbf{X}$ and $\mathbf{x}$, respectively. The displacement of the surface is denoted by $\mathbf{u}$ with relation $\mathbf{x}$=$\mathbf{X}$+$\mathbf{u}$.

The surface undergoes deformation described by the deformation gradient $\mathbf{F}$ which is given by $\mathbf{F} = \mathbf{I} + \frac{\partial \mathbf{u}}{\partial \mathbf{X}}$, where $\mathbf{I}$ is the identity tensor. Green-Lagrange strain tensor $\mathbf{E}$ is given by $\mathbf{E} = \frac{1}{2}\left(\mathbf{F}^T\mathbf{F} - \mathbf{I}\right)$. The excess of elastic strain energy near the surface can be written as

$$W^{ex} = A_0\Gamma \tag{1}$$

where A_0 is the surface area in the undeformed configuration and Γ is the Lagrangian surface excess energy (or excess elastic strain energy density). Now we define the second Piola-Kirchhoff surface stress tensor as follow;

$$\mathbf{S}^s = \frac{1}{A_0}\frac{\partial W^{ex}}{\partial \mathbf{E}} \tag{2}$$

By substituting Eq. (1) in (2), the surface stress can be written ;

$$\mathbf{S}^s = \frac{\partial \Gamma}{\partial \mathbf{E}} \tag{3}$$

This is the definition of surface stress which is based on Lagrangian framework. The surface elastic constants can be obtained as

$$\mathbf{C}^s_{ijkl} = \frac{\partial \mathbf{S}^s_{ij}}{\partial \mathbf{E}_{kl}} = \frac{1}{A_0}\frac{\partial^2 W^{ex}}{\partial \mathbf{E}_{ij}\partial \mathbf{E}_{kl}}, \quad i,j,k,l = 1,2,3. \tag{4}$$

and in terms of surface energy (on using Eq. (1)) as

$$\mathbf{C}^s_{ijkl} = \frac{\partial^2 \Gamma}{\partial \mathbf{E}_{ij}\partial \mathbf{E}_{kl}} \tag{5}$$

The surface elastic constant can be positive or negative [20].

III. SURFACE STRESS EFFECTS ON BENDING STIFFNESS AND RESONANCE FREQUENCY OF NANOCANTILEVERS

Nanostructures can be modeled using a continuum mechanics framework following the idea that "nanostructure=bulk+surface". The total energy of the cantilever can be written as

$$U = U_b + U_s \tag{6}$$

The strain energy of bulk, U_b, in the beam is given by

$$U_b = \int_0^L \int_A \frac{1}{2}\sigma_{xx}\varepsilon_{xx} dA dx \tag{7}$$

where A is the cross-sectional area of the uniform beam, L the length of the beam, σ_{xx} the axial stress, and ε_{xx} the normal strain. Using the linear strain-displacement relation

$$\varepsilon_{xx} = \frac{\partial u}{\partial x} = -z\frac{d^2 w_0}{dx^2} \tag{8}$$

we obtain

$$\begin{aligned} U_b &= \int_0^L \int_A \frac{E}{2}\left(-z\frac{d^2 w_0}{dx^2}\right)^2 dA dx \\ &= \int_0^L \frac{EI}{2}\left(\frac{d^2 w_0}{dx^2}\right)^2 dx \end{aligned} \tag{9}$$

where z is the coordinate in the load direction with the origin in the centroid of the cross section. The total surface free energy, U_s, at the entire beam surface is

$$\begin{aligned} U_s &= 2\int_s (\gamma(\varepsilon) - \gamma(0))\, ds = 2\int_s \frac{1}{2}C\varepsilon^2 ds \\ &= \int_0^L Cbt^2\left(\frac{d^2 w_0}{dx^2}\right)^2 dx \end{aligned} \tag{10}$$

where C is the surface elasticity, b is the width of the cantilever, and t is the thickness of the cantilever, respectively. The total energy of the beam would be

$$\begin{aligned} U &= \int_0^L \frac{EI}{2}\left(\frac{d^2 w_0}{dx^2}\right)^2 dx + \int_0^L Cbt^2\left(\frac{d^2 w_0}{dx^2}\right)^2 dx \\ &= \int_0^L \left(\frac{EI}{2} + Cbt^2\right)\left(\frac{d^2 w_0}{dx^2}\right)^2 dx \end{aligned} \tag{11}$$

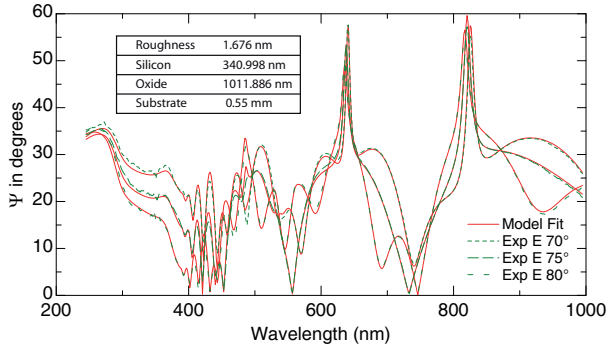

FIG. 2: Ellipsometer fitting result of the 340 nm SOI with different incident angles.

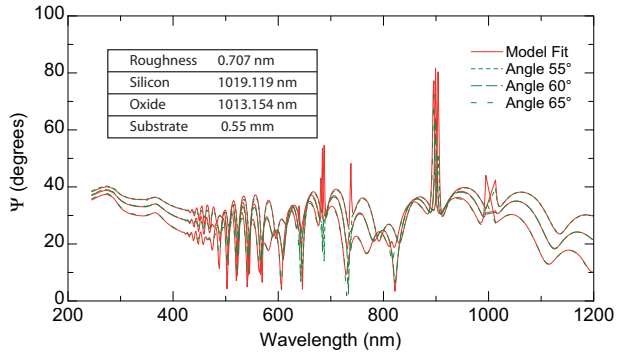

FIG. 3: Ellipsometer fitting result of the 1 μm epitaxy SOI with different incident angles. Shown on the inset is the resultant stack thickness of each layer. The roughness layer simulates the surface roughness of the wafer.

By comparing Eqs. (9) and (11), the effective bending stiffness to be used in the equations of motion can be obtained as

$$\frac{1}{2}(EI)^* = \frac{1}{2}\left(EI + Cbt^2\right) \tag{12}$$

Therefore, the change in the resonance frequency due to surface stress can be calculated as;

$$\frac{\omega^2 - \omega_0^2}{\omega_0^2} = \frac{E^* - E}{E} = \frac{6C}{Et} \tag{13}$$

where ω_0 is the fundamental resonance frequency without surface stress and ω is the new resonance frequency with the effect of surface stress. It is clear from Eq. (13) that the effect of surface stress depends on the thickness of the cantilever.

IV. FABRICATION OF SINGLE CRYSTALLINE SILICON CANTILEVERS

The single crystalline silicon cantilevers in this work are fabricated based on (100) silicon on insulator wafers from Soitech, using Smartcut® process to form the buried oxide and the silicon device layer. The wafers are shipped with 1 μm (measured 1012 nm) thick buried oxide and 340 nm thick silicon device layer. Figure 2 shows the thickness measurement by elipsometry for 340 nm thick SOI wafer.

For the 1μm thick cantilevers, the original SOI wafer is epitaxy grown with 660 nm of Si; a rapid high temperature treatment is first applied to clean and remove the native oxide before the epitaxy to ensure a continuous single crystalline layer growth. The layers are measured with ellipsometry and a pre-defined model is fitted onto the measured data to obtain the exact thicknesses. The fitting and its result is shown in Fig. 3, the difference between the measured data and the fitting has a mean square error (MSE) of 78, which is acceptable for complex thick layers. To further guarantee the quality of the epitaxy, we measure the surface roughness of the sample using AFM and obtain an atomic flatness (Fig. 4); this indicates a growth of single crystalline silicon instead of poly or amorphous silicon.

For the 100 nm thick cantilever, another SOI wafer is used and sent directly to a dry thermal oxidation furnace to consume 240 nm of the original Si. The wafer is then measured and fitted in the ellipsometer as shown in Fig. 5 and fitting of MSE 18 was obtained.

The (100) oriented cantilevers are patterned and released using surface micromachining processes shown in Fig. 6; samples with desired thickness are spin coated with photoresist and patterned in lithography step (Fig. 6(a)). The sample is then etched in a SF_6 based plasma etcher to pattern the top silicon layer until reaching the buried oxide (Fig. 6(b)). To release the cantilever, the residue of photoresist is removed in nitric acid and the buried oxide is etched in HF solution, the sample is then dried using critical-point-drying (CPD) technique, which prevents device stiction [17] (Fig. 6(c)). Fig. 7 shows the released and unreleased cantilevers. The cantilever bases have undercut geometries resulted from isotropic HF etching.

V. MEASUREMENT SETUP

The resonance behavior of the silicon cantilevers is measured in a home-made optical laser deflection setup operating in atmospheric and low vacuum environment (10^{-3} mbar). Fig. 8 depicts the configuration of the setup. The deflection of the cantilevers due to thermal noise is probed by a 658 nm laser diode. The output signal, the voltage difference generated by the reflected light focused on a two-segment diode, is measured with a spectrum analyzer to obtain thermal noise spectra. The laser spot is typically positioned at the end of the cantilever with a spot diameter of 6 μm and a power of a few mW. The electronic bandwidth of the setup is 5 MHz and its sensitivity is estimated to be about 1 pm/(Hz)$^{1/2}$. We have reduced the laser power by a factor of two and found that the noise spectra are not affected. Therefore, the measured spectra are attributed to thermal fluctuations and not to excitations induced by the laser light.

Thermal noise spectra can be measured for a large number of cantilevers with varying length (L) and thickness (t). The resonance frequency and the Q-factor of the resonances are determined from Lorentzian fits (red lines) through the data, as is illustrated in Fig. 9 for the first

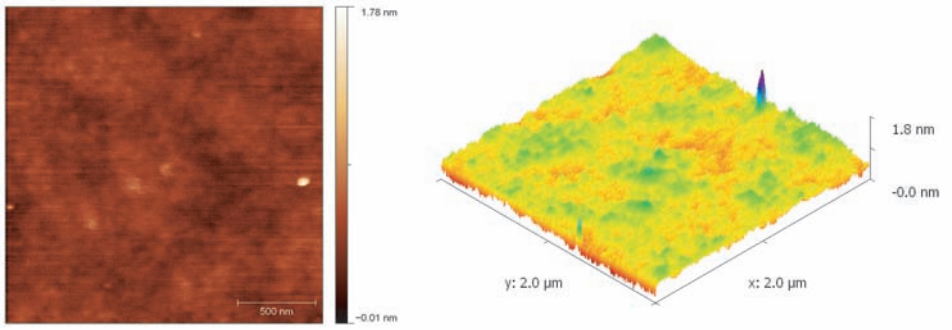

FIG. 4: Contact mode AFM of the 1μm epitaxy surface. The smooth surface indicates a continuous single crystalline growth from the original surface. The RMS of the surface is measured to be 0.095 nm.

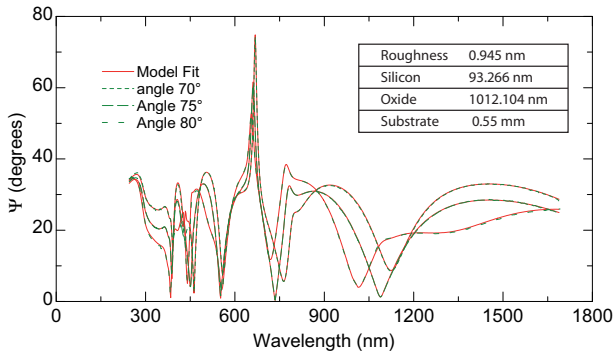

FIG. 5: Ellipsometer fitting result of the 93 nm oxidized and etched SOI with different incident angles. Shown on the inset is the resultant stack thickness of each layer.

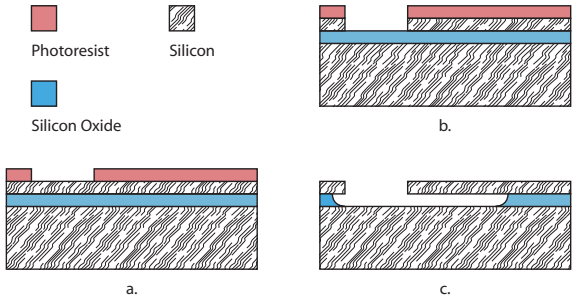

FIG. 6: Fabrication process of the cantilevers. Photoresist is patterned on the desired sample. Using the photoresist as etching mask, the silicon underneath is etched with SF_6 plasma. Residue of the resist is stripped in nitric acid and device submerged in HF solution to etch oxide. Device is put in CPD to release the suspending cantilever structure.

bending mode both in vacuum and in air for 93 nm-thick cantilever.
Fig. 10 shows data obtained from measuring cantilevers of different length in air and vacuum; the resonance frequency vs. length relation follows the well known $1/L^2$ trend.

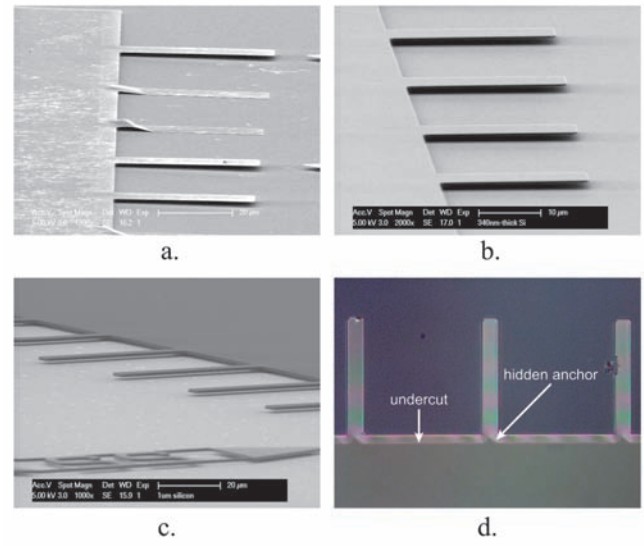

FIG. 7: (a), (b), (c): Fabrication result of the 93 nm, 340 nm and 1 μm thick cantilevers respectively. Stiction occurs after the etching of oxide in HF where CPD is needed to increase the yield in the releasing. Shown in (d) is the undercut of the cantilevers, it is the real fix end of the cantilever and has a lengthening effect on the device. Furthermore, a hidden anchor geometry is present at the cantilever base.

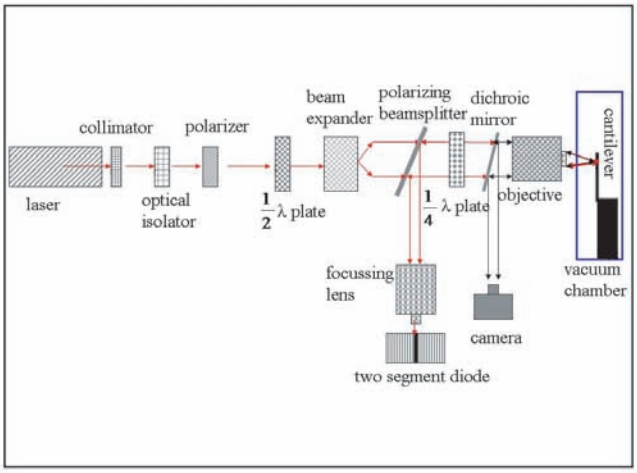

FIG. 8: Schematic of the optical deflection setup.

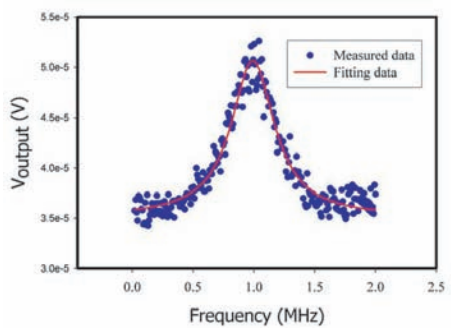

(a) Air

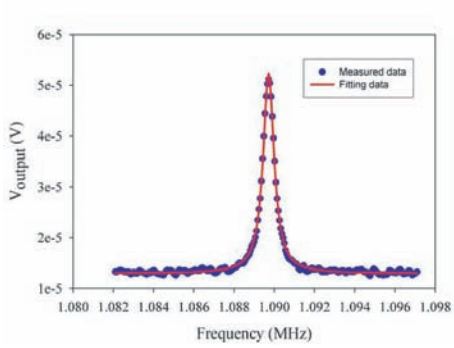

(b) Vacuum

FIG. 9: Resonance frequency peak of 93 nm-thick cantilever in air and vacuum.

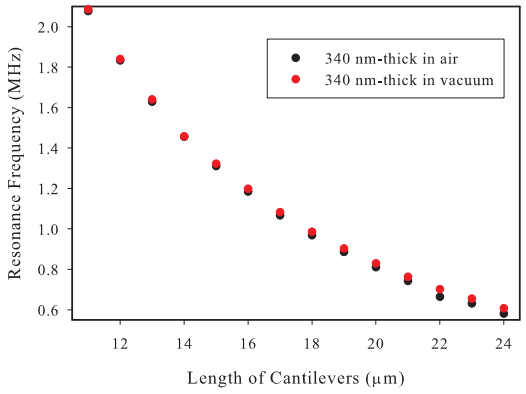

FIG. 10: Resonance frequency versus length of cantilevers.

VI. RESULTS AND DISCUSSION

To estimate the magnitude of $\Delta\omega$ we consider a silicon cantilever. Atomistic simulation for the Si (100) surface showed that $C \approx 11.5N/m$ [18, 19]. Table I shows the theoretical value obtained by classical beam theory, measured data in vacuum, in air, and the calculated resonance frequency affected by surface stress from Eq. (13) for different thicknesses of the cantilevers. Undercuts were taken into account in the calculations of the theoretic values, the lengthening effect was studied in [21]. The resonance frequency shift due to the hidden anchor was shown to be negligible [21]. Figure 9 shows the resonance peak of 93 nm-thick and 8 μm long cantilever in air and in vacuum.

It can be seen from the table that by scaling down the thickness of the cantilever, the effect of surface stress becomes significant. Since the measurement was carried out in vacuum, the water or/and gas adsorption at the surface of the cantilever was minimized. The difference between calculated results and measured data can be due to surface oxidation or other external effects caused by the environment. From the framework discussed in sections II and III, we know that the surface stress effect is a fundamental and intrinsic effect that is caused by the unavoidable self-reconstruction and relaxation of the atoms on the surface; it is size dependent and will become dominant as the device dimensions scale down. On the other hand, the surface stiffening due to oxidation and adsorption that is observed in our measurements, are considered to be external, or additional effects; these effects cause dominant shifts in resonance frequency and change the response of nanocantilevers, but are considered to be avoidable or can be minimized.

VII. CONCLUSION

In this paper, we developed a new framework that includes the effect of surface stress on resonance frequency of nanocantilevers. We showed in theory that surface stress can cause a significant difference in resonant frequency compared to the value obtained by classical beam theory. Furthermore, we fabricated single crystalline silicon cantilevers of different thicknesses and measured their resonance frequencies; we showed that if the size of the cantilever is reduced to the nano-scale range, the surface stress effects, the surface oxidations and adsorption of gas or contaminants on mechanical behavior will become dominant and will have to be addressed carefully in future works. Finally, what our surface stress framework derived is an intrinsic property of a device; this effect is unavoidable and is fundamentally different from surface stiffening caused by external conditions, or interactions between the device and its environment.

Acknowledgments

This work was done as part of Dutch national research program on micro technology, MicroNed (Project code: IV-C-2).

TABLE I: resonance frequency of cantilevers with different dimensions. resonant data are in KHz.

Dimensions $(L\times b\times t)$ μm^3	ω_0	$\omega_{measured}$ (vacuum)	$\omega_{measured}$ (air)	ω_{stress}
100×8×1.024	129.61	136.024	132.400	129.64
19×8×0.340	884.23	902.664	885.253	884.76
19×8×0.093	241.86	269.92	136.71	242.39
8×8×0.093	888.51	1089.72	986.767	890.46

References

[1] B. Ilic and H. G. Craighead, J. Appl. Phys. **95**, 3694 (2004).

[2] A. Gupta, D. Akin, and R. Bashir, Appl. Phys. Lett. **84**, 1976 (2004).

[3] M. Su, S. Li, and V. P. Dravid, Appl. Phys. Lett. **82**, 3562 (2003).

[4] Z. Shen, W. Y. Shih, and W. Shih, Appl. Phys. Lett. **89**, 023506 (2006).

[5] T. Thundat, E. A. Wachter, S. L. Sharp, and R. J. Warmack, Appl. Phys. Lett. **66**, 1695 (1995).

[6] G. Y. Chen, T. Thundat, E. A. Wachter, and R. J. Warmack, J. Appl. Phys. **77**, 3618 (1995).

[7] M. J. Lachut and J. E. Sader, Phys. Rev. Lett. **99**, 206102 (2007).

[8] J. Fritz, M. K. Baller, H. P. Lang, H. Rothuizen, P. Vettiger, E. Meyer, H. J. Guntherodt, Ch. Gerber, and J. K. Gimzewski, Science **288**, 316 (2000).

[9] J. H. Lee, K. H. Yoon, and T. S. Kim, Appl. Phys. Lett. **84**, 3187 (2004).

[10] Y. Zhang, Q. Ren, and Y.-P. Zhao, J. Phys. D **37**, 2140 (2004).

[11] K. S. Hwang, K. Eom, J. H. Lee, D. W. Chun, B. H. Cha, D. S. Yoon, T. S. Kim, and J. H. Park, Appl. Phys. Lett. **89**, 173905 (2006).

[12] A. W. McFarland, M. A. Poggi, M. J. Doyle, L. A. Bottomley, and J. S. Colton, Appl. Phys. Lett. **87**, 053505 (2005).

[13] J. Dorignac, A. Kalinowski, S. Erramilli, and P. Mohanty, Phys. Rev. Lett. **96**, 186105 (2006).

[14] G.-F. Wang and X.-Q. Feng, Appl. Phys. Lett. **90**, 231904 (2007).

[15] P. Lu, S. J. O'Shea, K. H. Lee, T. Y. Ng, Mater. Phys. Mech. **4**, 51 (2001).

[16] Q. Ren and Y.-P. Zhao, Microsystem Technologies **10**, 307 (2004).

[17] G. T. Mulhern, D. S. Soane, and R. T. Howe, Digest. Tech. Papers, 7th Int. Conf. Solid-State Sensors and Actuators (transducers '93, Yokohama) pp296-9, 1993.

[18] R. E. Miller and V. B. Shenoy, Nanotechnology **11**, 139 (2000).

[19] J. Zang, M. Huang, and F. Liu, Phys. Rev. Lett. **98**, 146102 (2007).

[20] L. G. Zhou and H. Huang, Appl. Phys. Lett. **84**, 1940 (2004).

[21] K. Babaei Gavan, E. W. J. M. van der Drift, W. J. Venstra, M. R. Zuiddam, and H. S. J. van der Zant, J. Micromech. Microeng. **19**, 035003 (2009).